JACS
JOURNAL OF THE AMERICAN CHEMICAL SOCIETY

pubs.acs.org/JACS

Article

Synthesis of Contorted Polycyclic Conjugated Hydrocarbons via Regioselective Activation of Cyclobutadienoids

Xianglin Yin,[†] Ke Zheng,[†] Zexin Jin, Matias Horst, and Yan Xia*

Cite This: *J. Am. Chem. Soc.* 2022, 144, 12715−12724

Read Online

ACCESS | Metrics & More | Article Recommendations | Supporting Information

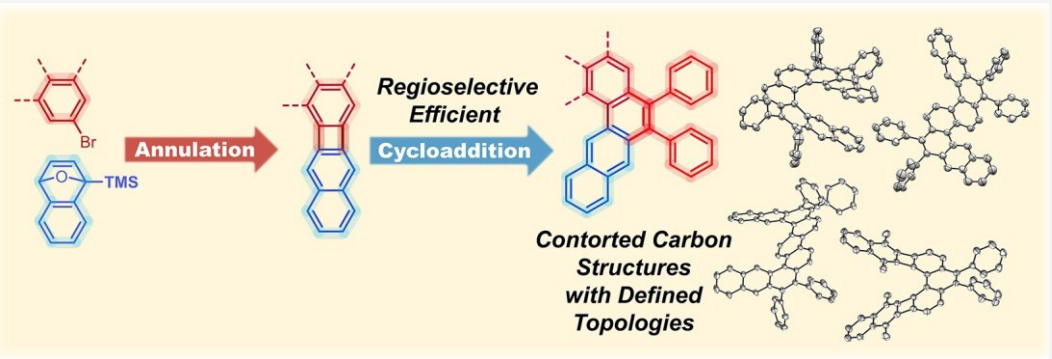

ABSTRACT: Contorted carbon structures have drawn much attention in the past decade for their rich three-dimensional geometries, enhanced solubility, and tunable electronic properties. We report a modular method to synthesize contorted polycyclic conjugated hydrocarbons containing helical moieties in controlled topologies. This strategy leverages our previously reported streamlined synthesis of π-systems containing four-membered cyclobutadienoids (CBDs), whose catalyzed cycloaddition with alkynes affords helical structures. Interestingly, we observed exclusive nonbay region regioselectivity in the C−C bond activation of CBDs in our system, which is opposite to the scarce previous examples of [*N*]phenylene activation that led to the formation of linear phenacene structures. The quantitative and regioselective nonbay region alkyne cycloaddition yielded a variety of helical carbon structures with their topologies predetermined by the CBD-containing precursor hydrocarbons. The cycloaddition can be inhibited by methyl substituents exocyclic to the four-membered ring, thus allowing selective activation of only certain desired CBD units while leaving the others intact. Calculation elucidated the basis for the observed regioselectivity. The described method provides a new route to multihelical aromatic hydrocarbons with complex yet defined geometries, facilitating the further exploration of such fascinating carbon structures.

INTRODUCTION

Polycyclic conjugated hydrocarbons (PCHs) are important functional nanocarbon materials for organic optical and electronic applications.[1−7] Introducing four-membered rings into PCHs imparts cyclobutadienoid (CBD) character, and the C−C bonds connecting the two adjacent benzenoids in the four-membered ring are relatively weak.[8] As a result, biphenylene, the simplest PCH containing a four-membered ring, can be activated by a range of metal catalysts via oxidative addition to form dibenzometallocycles.[9−14] Previous studies have demonstrated the possibility of catalyzed cycloaddition of biphenylene with π-bonds, such as alkynes and alkenes.[9,15−17] However, only two reports describe the activation of PCHs larger than biphenylene containing more than one four-membered ring.[18,19] Vollhardt and co-workers reported alkyne cycloaddition to angular [3] and [4]phenylenes, which contain 3 and 4 benzenoids, respectively, that are fused with four-membered rings, and the cycloaddition occurred selectively in the bay region (the inner rim of angular [*N*]phenylenes) to produce phenacene structures in moderate yields (Scheme 1a), and a mixture of singly and multiply activated products was observed.[18] Kotora and co-workers reported Iridium-catalyzed cycloaddition of various alkynes to biphenylene, and double cycloaddition to [3]phenylenes also yielded [5]phenacene in relatively low yields as a result of bay region cycloaddition (Scheme 1a).[19] Alternatively, if the alkyne insertion could occur in the nonbay region, helical benzo-phenathrene structures would be formed (Scheme 1b). Curved or contorted PCHs have captivated increasing interest due to their enhanced solubility and thus processability compared to planar

Received: March 6, 2022
Published: July 6, 2022

© 2022 American Chemical Society

https://doi.org/10.1021/jacs.2c02457
J. Am. Chem. Soc. 2022, 144, 12715−12724

Scheme 1. Opposite Regioselectivity in Alkyne Cycloaddition to [3]phenylene (a) and PCHs Described in This Work (b) Leads to Topologically Different Products

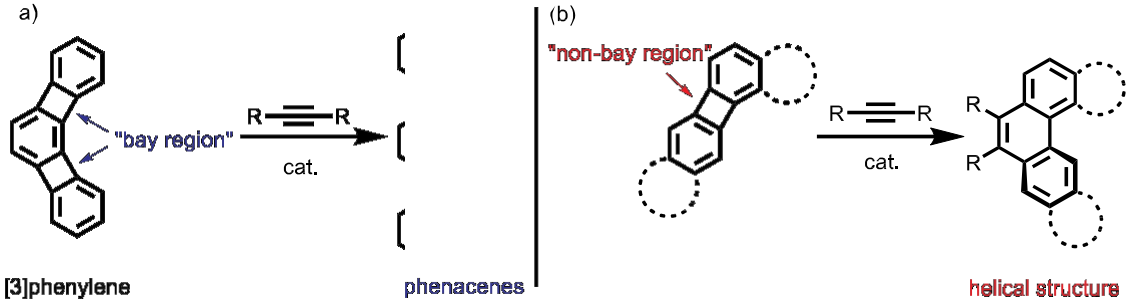

carbon structures, rich chiral geometries that serve as structural elements for more complex three-dimensional topologies of carbon structures, and tunable optoelectronic properties and functions.[20−31] Thus, modular and efficient chemistry to synthesize curved nanocarbon structures is highly desired.

Our group has recently developed an efficient method to access a variety of CBD-containing PCHs, using bromoarenes and benzooxanorbornadienes (oNBEs) as building blocks.[32−36] In this synthetic strategy, catalytic arene-(oxa)-norbornene annulation (CANAL) between bromoarenes and oNBEs yielded annulated areno-cyclobutene structures, which can be then aromatized under acidic conditions to generate PCHs containing fused CBDs. Herein, we report an efficient and completely selective nonbay region alkyne cycloaddition into various PCHs containing CBDs, giving rise to a diverse range of curved conjugated structures with new and predefined topologies. Further, we discovered that substitution exocyclic to a CBD prevents its activation, and thus, desired CBDs can be selectively activated or preserved in PCHs containing multiple CBD rings using strategically designed substitution.

RESULTS AND DISCUSSION

Synthesis of Nonsubstituted CBD-Containing PCHs. In our previously reported CANAL reactions, dimethyl substitution at the bridge head positions of oNBEs was required to prevent an undesired ring-opening reaction of oNBEs and facilitate the aromatization.[32] However, this requirement constrains the design of PCH structures. Additionally, in our preliminary study, we have found that the synthesized PCHs with the methyl substituents exocyclic to the CBD cannot be activated by common transition-metal catalysts known to activate biphenylene (Scheme S1). To circumvent this constraint and bestow the design freedom, we sought a removable substitution strategy, where the substituent must be tolerated under CANAL conditions and easily removed during the aromatization step. The trimethylsilyl (TMS) group is the desired candidate since it satisfies these criteria and is easy to install and remove. We first synthesized benzooxanorbornadiene 1 containing a TMS substituent at one bridge head position. Model CANAL reaction between 1 and bromobenzene was conducted using our previously reported conditions, 5 mol % $Pd(OAc)_2$, Johnphos ligand, and Cs_2CO_3; however, no desired annulated product was observed while most of the starting materials have been consumed. Inspired by a report by Zhou and co-workers on annulation between norbornene and aryl halides using NaOPh as the base,[37] we attempted new conditions using 10 mol % $Pd(OAc)_2$, 20 mol % tBu$_3$P·HBF$_4$, and 1.5 equiv. NaOPh (entry 1, Table 1) and obtained a 34% yield of the desired product for the model reaction. After exploring a few conditions with different Pd sources and ligands (entries 2−5 in Tables 1 and S1), we found that using 10 mol % $Pd(acac)_2$, 20 mol % tBu$_3$P·HBF$_4$, and 1.5 equiv. NaOPh gave the highest yield of 74% among the explored conditions. Changing the Pd source to $Pd(PPh_3)_4$ or changing the base to Cs_2CO_3 gave little or no desired product, respectively (entries 5−6, Table 1). Using the optimized conditions, we synthesized 3b−e (Table 2) via CANAL between 1 and 1-bromonaphthalene, 2-bromonaphthalene, 1-bromo-7-t-butylpyrene, and 9-bromophenanthrene, respectively, in 34−76% yields. Satisfyingly, we also synthesized more extended CANAL products

Table 1. Optimization of Palladium-Catalyzed CANAL between TMS-oNBE 1 and Bromobenzene

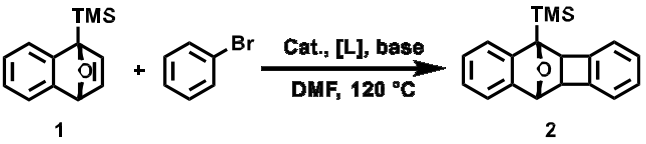

entry	cat.	[L]	base	yield (%)[a]
1	$Pd(OAc)_2$	tBu$_3$P·HBF$_4$	NaOPh	34
2	$Pd(acac)_2$	tBu$_3$P·HBF$_4$	NaOPh	74
3	$Pd(acac)_2$	Johnphos	NaOPh	45
4	$Pd(acac)_2$	PCy_3	NaOPh	34
5	$Pd(PPh_3)_4$		NaOPh	9
6	$Pd(acac)_2$	tBu$_3$P·HBF$_4$	Cs_2CO_3	0

[a]Based on ^{1}H NMR integration against an internal standard.

Table 2. Synthesis of Unsubstituted CBD-Containing PCHs

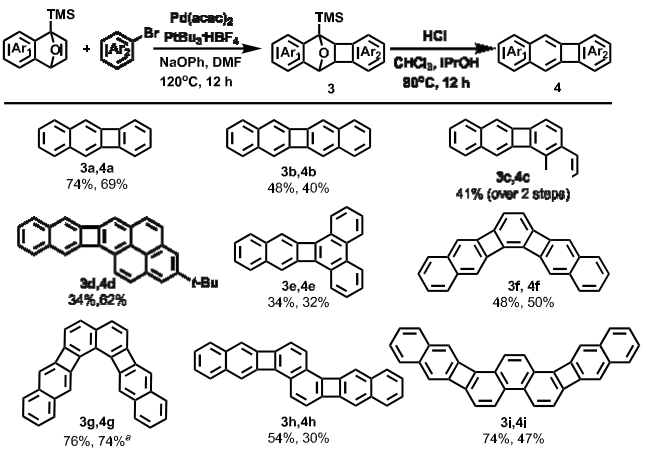

[a]Conditions: HCl, toluene/EtOH, 80 °C, 12 h.

https://doi.org/10.1021/jacs.2c02457
J. Am. Chem. Soc. 2022, 144, 12715−12724

3f−i (Table 2) containing two four-membered rings in 48−76% yields, using 1,2-dibromobenzene, 1,8-dibromonaphthalene, 1,5-dibromonaphthalene, and 1,8-dibromophenanthrene, respectively, as the starting materials. With the TMS-substituted CANAL products 3a−i on hands, we aromatized them under acidic conditions, using concentrated HCl in *i*PrOH/$CHCl_3$ at 80 °C. Delightfully, aromatization was achieved with simultaneous removal of the TMS group to yield unsubstituted PCHs in 30−74% yields. Pure products 4a−g (Table 2) were isolated by filtration after precipitation in methanol or column chromatography. For 4g, using concentrated HCl in toluene/ethanol at 80 °C increased the yield from 30 to 74%. 4h and 4i exhibited sparse solubility in common nonpolar solvents even at elevated temperatures, and their crude products were used for the subsequent alkyne cycloaddition (*vide infra*). The V-shaped 4g is a new regioisomer of the [3]naphthylene family that we have previously reported.[33] Interestingly, 4g has significantly enhanced solubility compared to the regioisomeric angular [3]naphthylene 4h. A detailed study of new [3]naphthylene isomers and effects of antiaromaticity will be reported in due course.

Regioselective Alkyne Cycloaddition. Vollhardt and Kotora have shown that angular [*N*]phenylenes can be transformed into phenacene structures via bay region alkyne cycloaddition.[18,19] With a series of new CBD-containing PCHs on hand, we studied their catalytic activation and alkyne cycloaddition. Using conditions identical to those reported by Kotora,[19] compounds 4a−d (Table 3) were reacted each with a stoichiometric (to CBD) amount of diphenylacetylene in the presence of 10 mol % $[Ir(cod)Cl]_2$, 20 mol % 1,2-bis(diphenylphosphino)ethne (dppe) in toluene at 130 °C for 18−36 h. Delightfully, a single product was obtained in nearly quantitative yields (95 to 98%) for each reaction. In contrast, compound 4b-Me_2 with two exocyclic methyl substituents did not undergo any reaction under the same conditions, suggesting that the absence of exocyclic substituents is important for successful CBD activation. Using dimethyl acetylenedicarboxylate or bis(trimethylsilyl)acetylene gave no or low conversion, presumably due to unfavorable electronics or steric hindrance, respectively. We then examined the regioselectivity of alkyne cycloaddition. The ^{1}H NMR spectrum of the activated product from the angular [2]-naphthylene 4c showed a singlet at 9.65 ppm and a doublet at 9.30 ppm (Figure 2a); the chemical shifts and the splitting pattern suggested a helical benzo[*a*]tetraphene moiety.[38] This molecular topology was further confirmed by the NOE experiment, which showed a clear correlation between protons H_1 and H_2 in the inner rim of 5c (Figure S1). The NMR experiments indicated exclusive nonbay region activation, leading to the formation of a helically contorted product. This is in stark contrast to the bay region selectivity observed in previous [*N*]phenylene activation, which results in a linear phenacene topology.[18,19] We also attempted the alkyne cycloaddition under identical conditions on compound 4e with a CBD-fused phenanthrene moiety, but 4e remained unreacted after 24 h, further suggesting that the observed activation only occurs at the nonbay region.

Study of the Regioselectivity for Nonbay Region Activation. We next set out to understand the observed opposite regioselectivity to that reported on the activation of [*N*]phenylene. The previous computational study of the catalytic activation of [*N*]phenylene showed that the first metal cycloaddition in the bay region formed a more stable transition state (TS) structure than the nonbay region cycloaddition, which was rationalized as the stabilization of

Table 3. Alkyne Cycloaddition of CBD-Containing PCHs

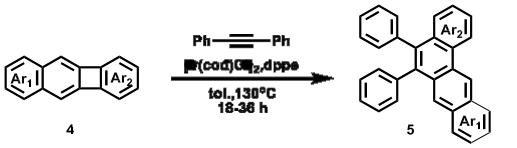

Substrate	Product	Yield %
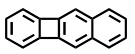 4a	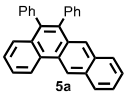 5a	87%
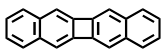 4b	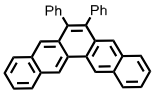 5b	98%
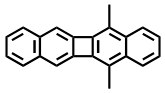 4b-Me_2	—	0%
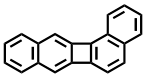 4c	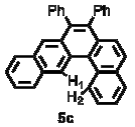 5c	95%
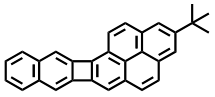 4d	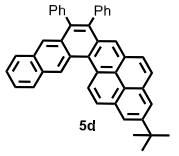 5d	96%
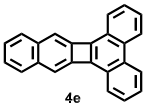 4e	—	0%
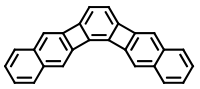 4f	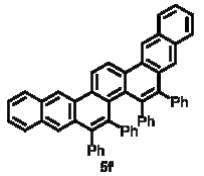 5f	50%
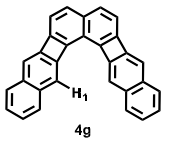 4g	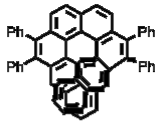 5g	85%
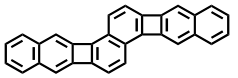 4h	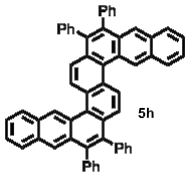 5h	61%
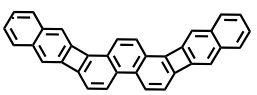 4i	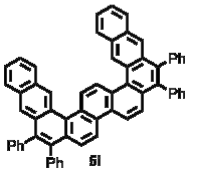 5i	67%

https://doi.org/10.1021/jacs.2c02457
J. Am. Chem. Soc. 2022, 144, 12715−12724

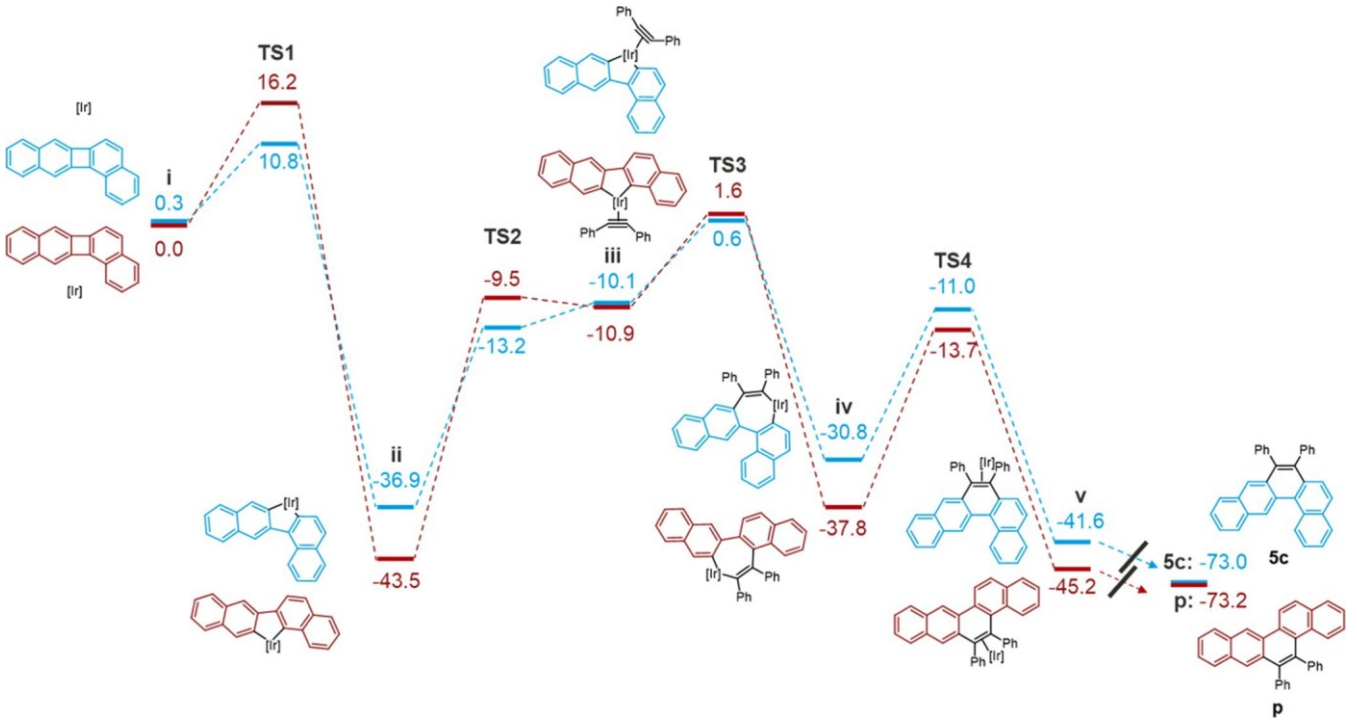

Figure 1. Free-energy profile and intermediates for the alkyne cycloaddition reaction of 4c with $[Ir(cod)Cl]_2$ and dppe, showing the observed nonbay addition pathway (blue) and the unobserved bay addition pathway (red). All energies (in kcal/mol) were calculated at the M06-2X/6-311++G(d,p)-SDD/SMD(toluene)//B3LYP/6-31G(d)-SDD level with free-energy corrections at 428 K and 0.2 M.

Scheme 2. Bay Region Cycloaddition for Compound 4f

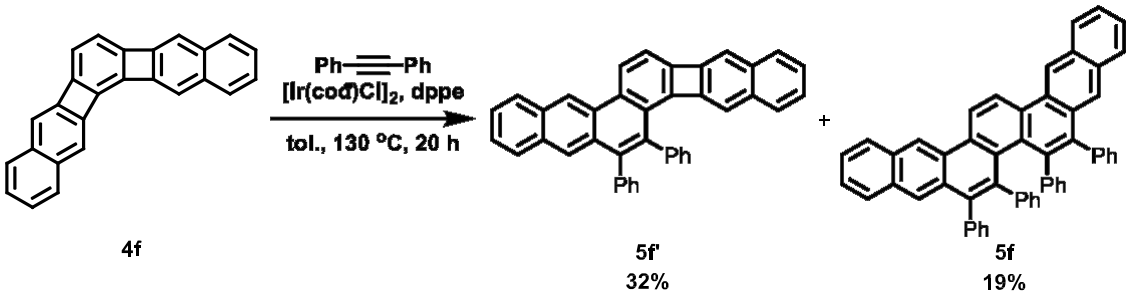

the polarized metal−carbon bond by the neighboring CBD ring.[18] However, the product via bay region alkyne cycloaddition has higher energy compared to the nonbay region cycloaddition product due to the steric hindrance of the phenyl substituents on one side of the formed phenacene structures. The second metal cycloaddition from the bay region is still favored due to the stabilization of the metal complex by the neighboring phenyl group from the first alkyne cycloaddition. Thus, the CBD activation of angular [*N*]phenylene is kinetically controlled with more stable TS in the generation of bay region cycloaddition intermediates.

To understand our observed nonbay region selectivity, we computationally investigated the Ir-catalyzed alkyne cycloaddition of angular [2]naphthylene. We determined the geometries and thermal free energies of the starting materials, key transition states, intermediates, and products of both bay and nonbay region reaction pathways using density functional theory at the B3LYP/6-31G(d)-Ir-SDD level, and then, single-point electronic energy corrections were obtained at the M06-2X/6-311++G(d,p)-Ir-SDD level (Figure 1). The irreversible oxidative addition step was determined to be rate limiting. The intermediate (ii in Figure 1) for the alkyne-bound Ir metallocycle from the bay region activation was 6.6 kcal/mol more stable than that from the nonbay region activation. However, the TS for nonbay oxidative addition (TS1 in Figure 1) is 5.4 kcal/mol more stable than that for bay oxidative addition, suggesting that the reaction selectivity is kinetically controlled in the oxidative addition of the Ir complex to [2]naphthylene. The free energies of the observed helical final product 5c and the unobserved zig-zag product p are identical. Therefore, the reaction kinetics rather than product thermodynamics play the determining role in the observed exclusive regioselectivity. The previously proposed stabilization of the metal complex by the neighboring CBD ring in angular [*N*]phenylene would not exist in our CBD-containing PCHs due to the long distance between CBD rings. We believe that this lack of stabilization of the metallocycle from the bay region activation primarily accounts for our observed opposite nonbay region activation, which is less sterically hindered.

To further test the hypothesis that the opposite regioselectivity is substrate-controlled, we synthesized a new substrate 4f via the CANAL method, featuring an angular

https://doi.org/10.1021/jacs.2c02457
J. Am. Chem. Soc. 2022, 144, 12715−12724

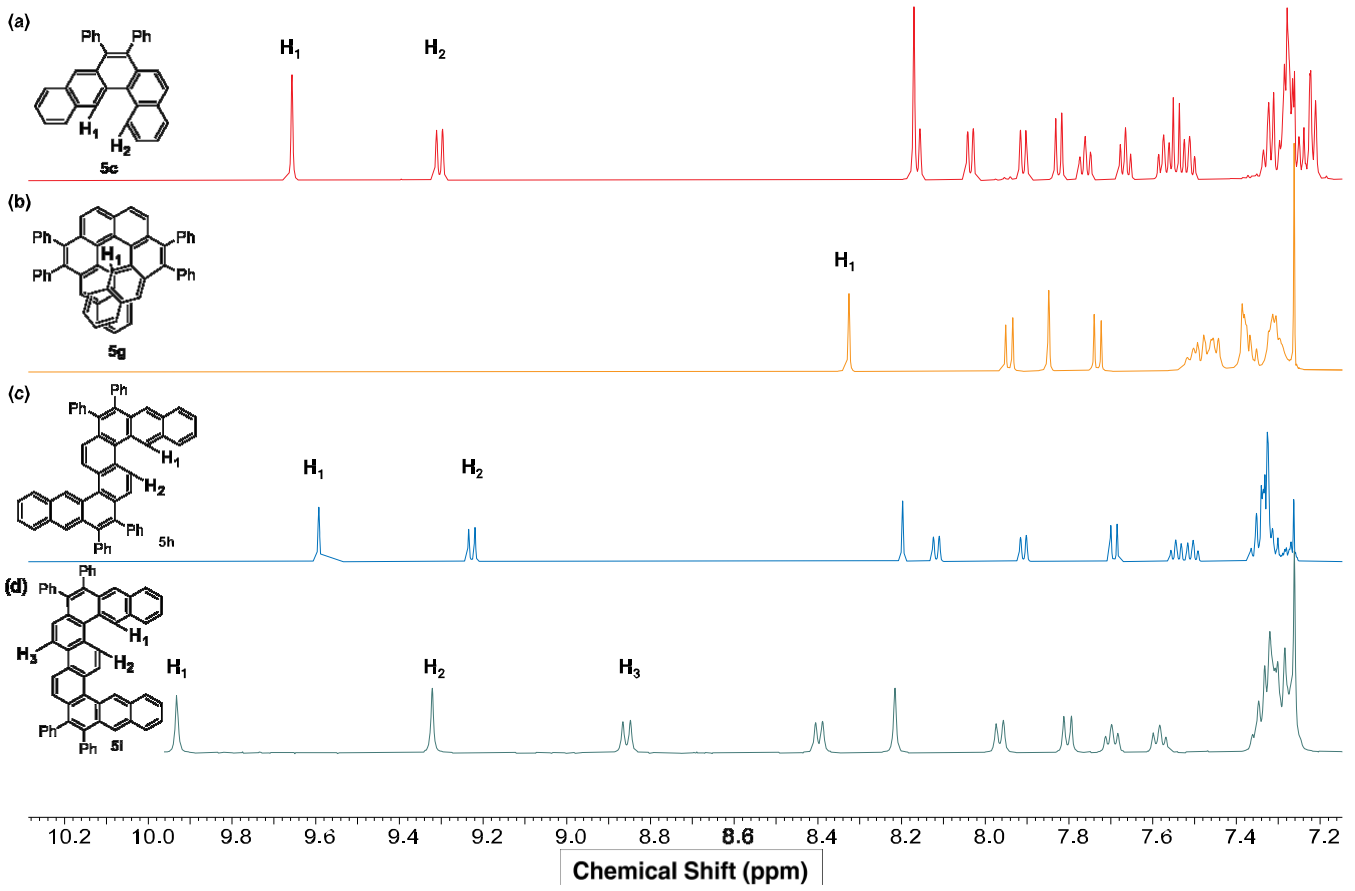

Figure 2. Partial ^{1}H NMR spectra of compounds 5c, 5g, 5h, and 5i.

[3]phenylene core structure that closely resembles the [3]phenylene substrate Vollhardt and Kotora have previously used. We performed the cycloaddition on 4f under identical conditions used for the substrates in Table 3. The activation of 4f proceeded much slower than the other substrates with only ~50% conversion by NMR spectroscopy after 20 h, resulting in a mixture of singly activated product 5f' and doubly activated product 5f (Scheme 2). Further prolonged reaction time led to alkyne trimerization and incomplete conversion of 4f (Table 3), which made the separation difficult. NMR spectra of the products agreed with those reported for [*N*]phenylene cycloaddition,[18,19] indicating the formation of phenacene structures. Thus, this observation suggests that the opposite cycloaddition regioselectivity is substrate-dependent and the proximity between CBD rings in [*N*]phenylenes (fused with one benzenoid in between) may account for the previously reported bay region selectivity and moderate yields using [*N*]phenylenes.

Synthesis of Helical PCHs via Multiple Regioselective Alkyne Cycloadditions. We further took advantage of the nonbay region regioselectivity to synthesize helical and curved carbon structures with defined topologies from extended CBD-containing PCHs by performing multiple alkyne cycloadditions. For V-shaped [3]naphthylene 4g, selective nonbay region alkyne cycloaddition cleanly produced a helical molecule 5g in 85% isolated yield (Table 3). Proton 1 (H_1) in 4g was shifted from 6.9 to 8.3 ppm (Figure 2b) upon alkyne cycloaddition, supporting the nonbay region activation to form a helical product structure.[38] Additionally, a group of new multiplets between 7.25 and 7.40 ppm was integrated into 20 protons, corresponding to the four phenyl substituents in the product 5g. These clear NMR features indicated the high efficiency and selectivity of the double nonbay region cycloaddition. For angular [3]naphthylene 4h, the alkyne cycloaddition proceeded regioselectively to generate an S-shaped core structure 5h as indicated by a singlet at 9.59 ppm and a doublet at 9.23 ppm (Figure 2c), similar to those observed in compound 5c (Figure 2a). Compound 4i also underwent clean nonbay region alkyne cycloaddition to yield a W-shaped molecule 5i (Figure 2d). Due to the very sparse solubility of 4h and 4i, the activation reaction began as a suspension but became a homogeneous solution within 18 h of the reaction and yielded significantly more soluble, doubly inserted pure products 5h and 5i in 61 and 67% yield, respectively, after column chromatography (Table 3).

Single crystals of 5g, 5h, and 5i suitable for X-ray diffraction were all obtained by slow diffusion of methanol into their chloroform solutions at 25 °C (Figures 3 and S2). Their crystal structures unambiguously proved the nonbay region selectivity and the curved structures of products. The structure of 5g can be seen as a [6]helicene core with two benzo groups fused at the C3−C32 and C19−C24 bonds. The twist angle of the helical turn (ring B to G) in 5g is measured to be 32.6°, smaller than that in [6]helicene (58.5°). The crystal structures of 5h and 5i show an S-shaped and a W-shaped topology, respectively. In 5h, the two terminal naphthalene wings are slightly twisted and both bend to the same side relative to the central chrysene with a twist angle of 35.2° between rings B and E. In 5i, the two terminal naphthalene wings also bend to the same side relative to the central picene with a slightly

https://doi.org/10.1021/jacs.2c02457
J. Am. Chem. Soc. 2022, 144, 12715−12724

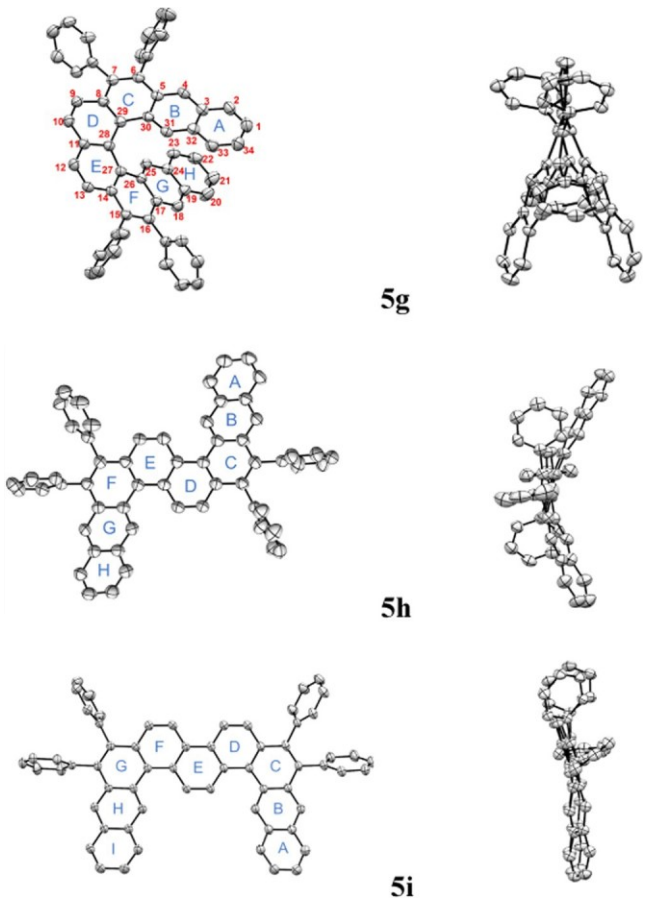

Figure 3. Single-crystal structures of 5g, 5h, and 5i resulting from exclusive nonbay region alkyne cycloaddition to the CBD-containing PCHs. Hydrogen atoms are omitted for clarity.

smaller twist angle of 29.1° between rings B and E. The degree of distortion in 5h and 5i is comparable to that in [4]helicene (27°).[39] These crystal structures confirmed that selective nonbay region CBD activation is a viable method to synthesize helical carbon structures.

The optical and redox properties of compounds 5g−i were investigated by UV−vis spectroscopy and cyclic voltammetry. 5g exhibited λ_{onset} at 461 nm, corresponding to an optical gap of 2.69 eV (Figures 4 and S3). 5h and 5i showed more blue-shifted λ_{onset} of 441 and 430 nm (Figures 4 and S3) with an optical gap of 2.80 and 2.89 eV, respectively. We also performed time-dependent density functional theory (TD-DFT) at the B3LYP/6-311+G* level of theory to calculate the highest occupied molecular orbital−lowest unoccupied molecular orbital (HOMO−LUMO) energy gaps to be 2.85, 2.75, and 2.87 eV for 5g, 5h, and 5i, respectively (Table 4), which are close to the measured optical gaps. The redox properties of 5g−i were also examined by cyclic voltammetry in dichloromethane (Figure S4). Within the solvent window, compound 5g showed multiple irreversible oxidation peaks, while 5h and 5i showed two reversible oxidation peaks. The first oxidation potential of 5g is at + 0.676 V (vs F_c/F_c^+), corresponding to a HOMO level of −5.48 eV. Similarly, the first oxidation potential of 5h and 5i was measured to be +0.658 and +0.735 V (vs F_c/F_c^+), respectively. The HOMO level of 5h and 5i was calculated to be −5.46 and −5.53 eV, respectively (Table 4).

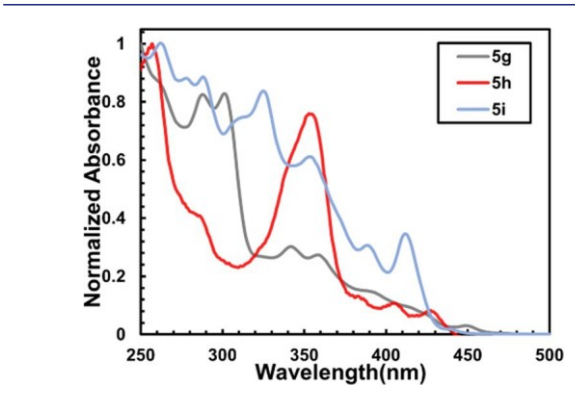

Figure 4. UV−vis spectra of 5g, 5h, and 5i in $CHCl_3$ solution.

Since we observed that exocyclic dimethyl substituents inhibit CBD activation, strategically designed substitution and nonsubstitution can be used to control the activation only for the desired CBD rings to further control the topology and electronic properties of the formed π-systems. To this end, we demonstrated selective CBD activation using a dibenzo[4]-phenylene 4j. CANAL reaction between 1,8-dibromobiphenylene and dimethyl oNBE under our previously reported conditions (20 mol % $Pd(acac)_2$ and 40 mol % JohnPhos, 4 equiv. Cs_2CO_3 in THF) furnished the desired doubly annulated product 3j in 30% isolated yield. Then, its aromatization using HCl in *i*PrOH/$CHCl_3$ gave 4j as a yellow precipitant in a 49% yield after filtration. 4j contains three CBD rings, and only the central CBD ring contains no exocyclic substitution (Figure 5a). Compound 4j showed λ_{onset} of 505 nm (Figure 6), corresponding to forbidden HOMO to LUMO + 1 and HOMO − 1 to LUMO transitions based on TD-DFT calculation.

Alkyne cycloaddition on 4j was performed using 2 equiv. diphenylacetylene in the presence of the 10 mol % $[Ir(cod)Cl]_2$, dppe ligand in toluene at 130 °C and gave 5j in a 47% yield after column chromatography (Figure 5a). Compared to 4j, 5j showed a blue-shifted λ_{onset} to 398 nm and significant changes in the absorption profile (Figure 6). Protons H_1 (6.57 ppm) and H_2 (6.45 ppm) in 4j were shifted to 7.10 and 7.03 ppm, respectively, in 5j (Figure 5b), while signals from the fused naphthalenoids and the two methyl substituents were slightly shifted upfield (Figure S5). New multiplet signals from 7.13 to 7.20 ppm were integrated into 10 protons. All of the spectroscopic evidence indicates that only the central CBD was activated while the side CBD units remained intact, despite the excess alkyne used, and the selective nonbay region activation resulted in a strained U-shaped structure. Single-crystal structure of 5j from X-ray crystallographic analysis confirmed its helical U-shape topology (Figure 7a), showing a dramatic deviation from planarity due to the steric repulsion between the inner methyl groups, whose respective carbon atoms are 4.12 Å apart. The inner rim of the molecule displays a helically curved shape. The central phenanthrene moiety is distorted from planarity with a measured dihedral angle (C8−C9−C10−C11) of 22.4° for the inner rim. The two CBD-fused naphthalenoid arms are bent in opposite directions away from the central phenanthrene plane about 22.0 and 33.2° relative to the phenanthrenoid plane. The naphthalenoid arms are also slightly twisted out of the plane due to the steric repulsion from the inner rim methyl substituents. Harmonic oscillator model of aromaticity (HOMA) analysis was used to quantify the degree of bond alternation.[40,41] Similar to what we have previously observed in [3]naphthylenes,[33] the B (or H)

https://doi.org/10.1021/jacs.2c02457
J. Am. Chem. Soc. 2022, 144, 12715−12724

Table 4. Optical, Electrochemical, and Computational Data for Compounds 5g, 5h, and 5i

	optical[a]			electrochemical[b]			calculation[c]	
compound	λ_{max} [nm]	λ_{onset} [nm]	E_{gap} [eV]	E_{ox} [V]	HOMO [eV]	LUMO [eV]	E_{gap} [eV]	oscillator strength
5g	451	461	2.69	0.676	−5.48	−2.79	2.85	0.0025
5h	429	441	2.80	0.658	−5.46	−2.66	2.75	0.251
5i	413	430	2.89	0.735	−5.53	−2.65	2.87	0.507

[a]Optical spectra were obtained in $CHCl_3$ solution at 298 K; the optical gap was estimated from the absorption edge (λ_{onset}). [b]Electrochemical data were obtained at a scan rate of 10 mV/s in DCM containing 0.1 M nBu$_4$NPF$_6$ using a glassy carbon working electrode and F_c^+/F_c as an external standard. HOMO and LUMO energy levels in eV were calculated from the reversible half-potential waves using the equation, HOMO = −(4.80 + E_{ox}), LUMO = HOMO + E_{gap}. [c]TD-DFT calculations were performed at the B3LYP/6-311+G* level of theory.

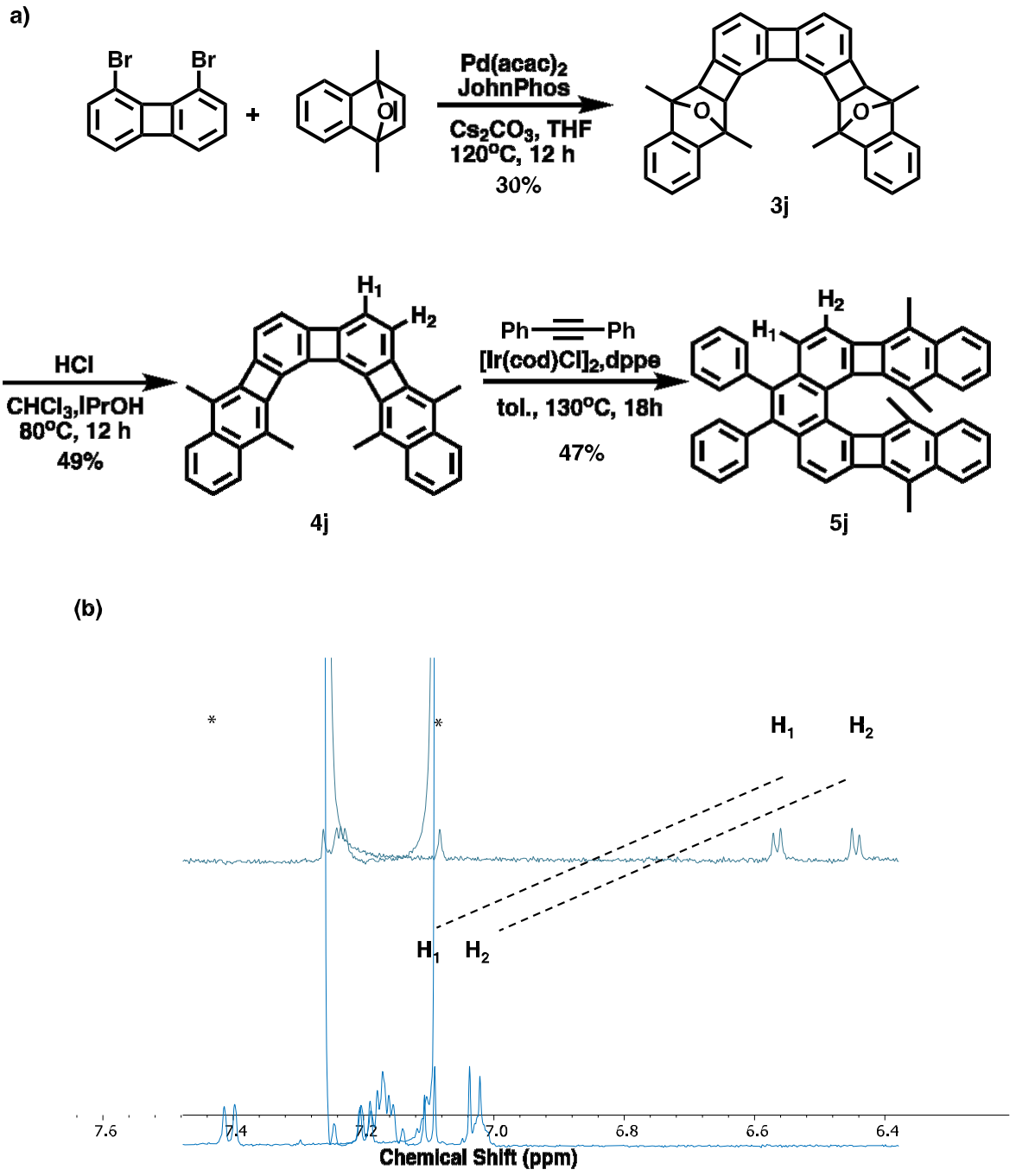

Figure 5. (a) Synthesis of angular dibenzo[4]phenylene and its selective alkyne insertion into the central CBD subunit. (b) Partial ^{1}H NMR spectra of compounds 4j and 5j.

https://doi.org/10.1021/jacs.2c02457
J. Am. Chem. Soc. 2022, 144, 12715−12724

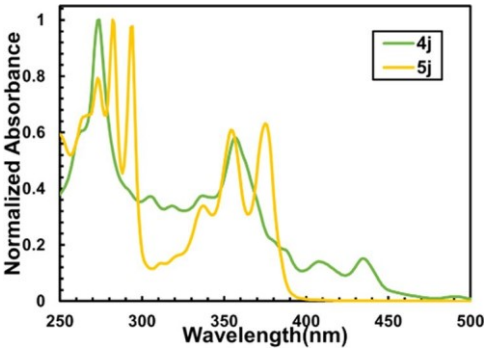

Figure 6. UV−vis spectra of 4j and 5j in $CHCl_3$ solution.

ring in terminal naphthalenoids has a HOMA value of 0.207 (Figure 7b) as compared to HOMA value of 0.736 in naphthalene and shows a strong propensity of bond alternation to minimize the antiaromaticity of CBD. The bond in the D ring that is fused to CBD is 1.411 Å long, longer than that in phenanthrene (1.381 Å), while the bonds exocyclic to CBD (inner rim C8−C9 = 1.393 Å and outer rim C30−C31 = 1.384 Å) are shorter than those in phenanthrene (1.413 and 1.406 Å, respectively). The E ring in phenanthrenoid has a HOMA value of 0.339 (Figure 7b) as compared to HOMA value of 0.455 in corresponding ring of phenanthrene and shows a distinct bond length difference between the C26−C27 bond (1.372 Å) and all of the other bonds (1.431−1.452 Å), suggesting π-bond localization at this bond as expected from a phenanthrene structure, but this bond is still longer than the corresponding bond in phenanthrene (1.357 Å). The CBD rings in 5j also exhibit interesting bonding asymmetry. The bond lengths of the CBD rings are all unequal. The inner rim C7−C8 bond is 1.512 Å long, longer than the outer rim C31−C32 bond, which is 1.489 Å long, presumably due to the steric repulsion imposed by the stacking methyl substituents. The C8−C31 bond (1.411 Å) fused to phenanthrenoid is shorter than the C7−C32 bond fused to naphthalenoid (1.449 Å). This example demonstrates the power of the presented synthetic strategy in accessing unusual curved PCHs with defined topologies. The remarkable regioselectivity is set by the topology of precursor molecules and the presence or absence of the exocyclic substitution of CBD rings.

CONCLUSIONS

In summary, we report a modular method to synthesize contorted conjugated hydrocarbons with defined and unprecedented topologies via highly efficient and regioselective alkyne cycloaddition into the nonbay regions of a variety of CBD-containing PCHs, which can be synthesized by our previously reported annulation chemistry in two steps from readily available arene building blocks. Further, it was found that the otherwise efficient alkyne cycloaddition can be inhibited by placing substitution exocyclic to the four-membered rings. The helical contorted PCHs are interesting structural elements for more complex three-dimensional carbon structures. Efforts are underway to apply this method to multialkyne structures and synthesize more extended contorted carbon structures, which will be reported in due course.

ASSOCIATED CONTENT

Supporting Information

The Supporting Information is available free of charge at https://pubs.acs.org/doi/10.1021/jacs.2c02457.

Experimental and computational details, ^1H and ^{13}C NMR spectra, UV−vis and CV characterizations, calculated band gaps, and computational results (PDF)

Accession Codes

CCDC 2095154−2095155, 2098285, and 2131192−2131193 contain the supplementary crystallographic data for this paper. These data can be obtained free of charge via www.ccdc.cam.ac.uk/data_request/cif, or by emailing data_request@ccdc.

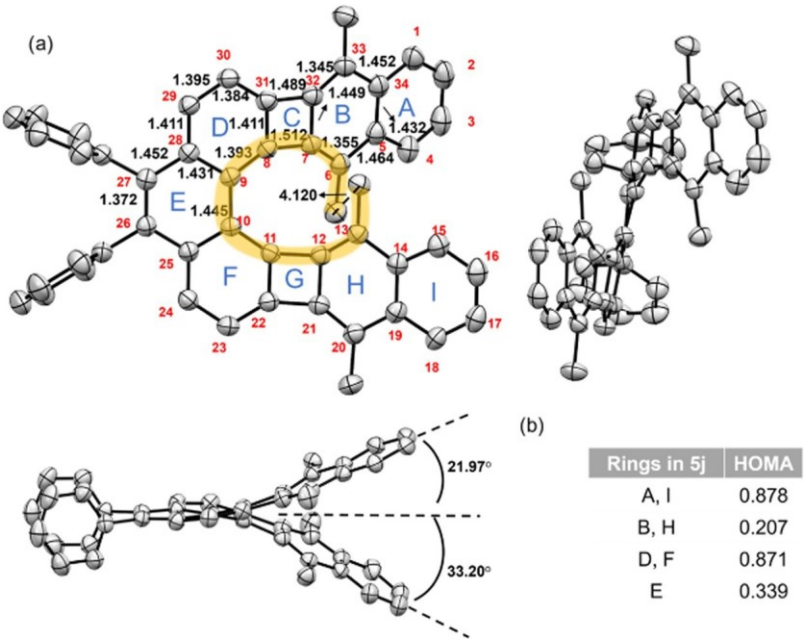

Figure 7. (a) X-ray crystal structure of 5j with top and side views. Hydrogen atoms are omitted for clarity. (b) Harmonic oscillator model of aromaticity (HOMA) for all of the rings in 5j.

https://doi.org/10.1021/jacs.2c02457
J. Am. Chem. Soc. 2022, 144, 12715−12724

cam.ac.uk, or by contacting The Cambridge Crystallographic Data Centre, 12 Union Road, Cambridge CB2 1EZ, UK; fax: +44 1223 336033.

AUTHOR INFORMATION

Corresponding Author

Yan Xia – *Department of Chemistry, Stanford University, Stanford, California 94305, United States;* orcid.org/0000-0002-5298-748X; Email: yanx@stanford.edu

Authors

Xianglin Yin – *Department of Chemistry, Stanford University, Stanford, California 94305, United States*

Ke Zheng – *Department of Chemistry, Stanford University, Stanford, California 94305, United States*

Zexin Jin – *Department of Chemistry, Stanford University, Stanford, California 94305, United States;* orcid.org/0000-0002-4971-3656

Matias Horst – *Department of Chemistry, Stanford University, Stanford, California 94305, United States;* orcid.org/0000-0002-9794-5355

Complete contact information is available at: https://pubs.acs.org/10.1021/jacs.2c02457

Author Contributions

†X.Y. and K.Z. contributed equally to this work.

Notes

The authors declare no competing financial interest.

ACKNOWLEDGMENTS

The authors thank the National Science Foundation for financial support (CHE-1855922) of this work. This research used resources of the Advanced Light Source, which is a DOE Office of Science User Facility under contract no. DE-AC02-05CH11231. M.H. is supported by a National Defense Science and Engineering Graduate Fellowship. The authors thank Prof. Yang Yang for the discussion of calculation. This work used the XStream computational resource, supported by the National Science Foundation Major Research Instrumentation program (ACI-1429830). Some of the computation was performed on the Stanford Sherlock cluster. The authors thank Stanford University and the Stanford Research Computing Center for providing computational resources and support that contributed to these research results.

REFERENCES

(1) Anthony, J. E. Functionalized Acenes and Heteroacenes for Organic Electronics. *Chem. Rev.* 2006, *106*, 5028−5048.
(2) Shen, Y.; Chen, C.-F. Helicenes: Synthesis and Applications. *Chem. Rev.* 2012, *112*, 1463−1535.
(3) Zhang, L.; Cao, Y.; Colella, N. S.; Liang, Y.; Brédas, J.-L.; Houk, K. N.; Briseno, A. L. Unconventional, Chemically Stable, and Soluble Two-Dimensional Angular Polycyclic Aromatic Hydrocarbons: From Molecular Design to Device Applications. *Acc. Chem. Res.* 2015, *48*, 500−509.
(4) Narita, A.; Wang, X.-Y.; Feng, X.; Mullen, K. New advances in nanographene chemistry. *Chem. Soc. Rev.* 2015, *44*, 6616−6643.
(5) Bunz, U. H. F. The Larger Linear N-Heteroacenes. *Acc. Chem. Res.* 2015, *48*, 1676−1686.
(6) Segawa, Y.; Ito, H.; Itami, K. Structurally uniform and atomically precise carbon nanostructures. *Nat. Rev. Mater.* 2016, *1*, 15002.
(7) Sun, Z.; Zeng, Z.; Wu, J. Zethrenes, Extended p-Quinodimethanes, and Periacenes with a Singlet Biradical Ground State. *Acc. Chem. Res.* 2014, *47*, 2582−2591.
(8) Takano, H.; Ito, T.; Kanyiva, K. S.; Shibata, T. Recent Advances of Biphenylene: Synthesis, Reactions and Uses. *Eur. J. Org. Chem.* 2019, *2019*, 2871−2883.
(9) Eisch, J. J.; Piotrowski, A. M.; Han, K. I.; Kruger, C.; Tsay, Y. H. Oxidative addition of nickel(0) complexes to carbon-carbon bonds in biphenylene: formation of nickelole and 1,2-dinickelecin intermediates. *Organometallics* 1985, *4*, 224−231.
(10) Schwager, H.; Spyroudis, S.; Vollhardt, K. P. C. Tandem palladium-, cobalt-, and nickel-catalyzed syntheses of polycyclic π-systems containing cyclobutadiene, benzene, and cyclooctatetraene rings. *J. Organomet. Chem.* 1990, *382*, 191−200.
(11) Lu, Z.; Jun, C.-H.; de Gala, S. R.; Sigalas, M.; Eisenstein, O.; Crabtree, R. H. Redox-active organometallic Ir complexes containing biphenyl-2,2′-diyl. *J. Chem. Soc., Chem. Commun.* 1993, *0*, 1877−1880.
(12) Perthuisot, C.; Jones, W. D. Catalytic Hydrogenolysis of an Aryl-Aryl Carbon-Carbon Bond with a Rhodium Complex. *J. Am. Chem. Soc.* 1994, *116*, 3647−3648.
(13) Lu, Z.; Jun, C.-H.; de Gala, S. R.; Sigalas, M. P.; Eisenstein, O.; Crabtree, R. H. Geometrically Distorted and Redox-Active Organometallic Iridium Complexes Containing Biphenyl-2,2′-diyl. *Organometallics* 1995, *14*, 1168−1175.
(14) Edelbach, B. L.; Lachicotte, R. J.; Jones, W. D. Mechanistic Investigation of Catalytic Carbon−Carbon Bond Activation and Formation by Platinum and Palladium Phosphine Complexes. *J. Am. Chem. Soc.* 1998, *120*, 2843−2853.
(15) Perthuisot, C.; Edelbach, B. L.; Zubris, D. L.; Simhai, N.; Iverson, C. N.; Muller, C.; Satoh, T.; Jones, W. D. Cleavage of the carbon−carbon bond in biphenylene using transition metals. *J. Mol. Catal. A: Chem.* 2002, *189*, 157−168.
(16) Takano, H.; Shiozawa, N.; Imai, Y.; Kanyiva, K. S.; Shibata, T. Catalytic Enantioselective Synthesis of Axially Chiral Polycyclic Aromatic Hydrocarbons (PAHs) via Regioselective C-C Bond Activation of Biphenylenes. *J. Am. Chem. Soc.* 2020, *142*, 4714−4722.
(17) Takano, H.; Kanyiva, K. S.; Shibata, T. Iridium-Catalyzed Formal [4 + 1] Cycloaddition of Biphenylenes with Alkenes Initiated by C-C Bond Cleavage for the Synthesis of 9,9-Disubstituted Fluorenes. *Org. Lett.* 2016, *18*, 1860−1863.
(18) Gu, Z.; Boursalian, G. B.; Gandon, V.; Padilla, R.; Shen, H.; Timofeeva, T. V.; Tongwa, P.; Vollhardt, K. P. C.; Yakovenko, A. A. Activated Phenacenes from Phenylenes by Nickel-Catalyzed Alkyne Cycloadditions. *Angew. Chem., Int. Ed.* 2011, *50*, 9413−9417.
(19) Korotvicka, A.; Císarová, I.; Roithová, J.; Kotora, M. Synthesis of Aromatic Compounds by Catalytic C-C Bond Activation of Biphenylene or Angular [3]Phenylene. *Chem. - Eur. J.* 2012, *18*, 4200−4207.
(20) Pascal, R. A. Twisted Acenes. *Chem. Rev.* 2006, *106*, 4809−4819.
(21) Pérez, E. M.; Martín, N. Curves ahead: molecular receptors for fullerenes based on concave−convex complementarity. *Chem. Soc. Rev.* 2008, *37*, 1512−1519.
(22) Bunz, U. H. F.; Menning, S.; Martín, N. para-Connected Cyclophenylenes and Hemispherical Polyarenes: Building Blocks for Single-Walled Carbon Nanotubes? *Angew. Chem., Int. Ed.* 2012, *51*, 7094−7101.
(23) Gingras, M. One hundred years of helicene chemistry. Part 1: non-stereoselective syntheses of carbohelicenes. *Chem. Soc. Rev.* 2013, *42*, 968−1006.
(24) Gingras, M.; Felix, G.; Peresutti, R. One hundred years of helicene chemistry. Part 2: stereoselective syntheses and chiral separations of carbohelicenes. *Chem. Soc. Rev.* 2013, *42*, 1007−50.
(25) Darzi, E. R.; Jasti, R. The dynamic, size-dependent properties of [5]−[12]cycloparaphenylenes. *Chem. Soc. Rev.* 2015, *44*, 6401−6410.
(26) Liu, J.; Li, B. W.; Tan, Y. Z.; Giannakopoulos, A.; Sanchez-Sanchez, C.; Beljonne, D.; Ruffieux, P.; Fasel, R.; Feng, X.; Mullen, K. Toward cove-edged low band gap graphene nanoribbons. *J. Am. Chem. Soc.* 2015, *137*, 6097−6103.
(27) Ball, M.; Zhong, Y.; Wu, Y.; Schenck, C.; Ng, F.; Steigerwald, M.; Xiao, S.; Nuckolls, C. Contorted Polycyclic Aromatics. *Acc. Chem. Res.* 2015, *48*, 267−276.

(28) Rickhaus, M.; Mayor, M.; Jurícek, M. Strain-induced helical chirality in polyaromatic systems. *Chem. Soc. Rev.* 2016, *45*, 1542−1556.
(29) Li, C.; Yang, Y.; Miao, Q. Recent Progress in Chemistry of Multiple Helicenes. *Chem. - Asian J.* 2018, *13*, 884−894.
(30) Majewski, M. A.; Stepien, M. Bowls, Hoops, and Saddles: Synthetic Approaches to Curved Aromatic Molecules. *Angew. Chem., Int. Ed.* 2019, *58*, 86−116.
(31) Kumar, R.; Aggarwal, H.; Srivastava, A. Of Twists and Curves: Electronics, Photophysics, and Upcoming Applications of Non-Planar Conjugated Organic Molecules. *Chem. - Eur. J.* 2020, *26*, 10653−10675.
(32) Jin, Z.; Teo, Y. C.; Zulaybar, N. G.; Smith, M. D.; Xia, Y. Streamlined Synthesis of Polycyclic Conjugated Hydrocarbons Containing Cyclobutadienoids via C−H Activated Annulation and Aromatization. *J. Am. Chem. Soc.* 2017, *139*, 1806−1809.
(33) Jin, Z.; Teo, Y. C.; Teat, S. J.; Xia, Y. Regioselective Synthesis of [3]Naphthylenes and Tuning of Their Antiaromaticity. *J. Am. Chem. Soc.* 2017, *139*, 15933−15939.
(34) Teo, Y. C.; Jin, Z.; Xia, Y. Synthesis of Cyclobutadienoid-Fused Phenazines with Strongly Modulated Degrees of Antiaromaticity. *Org. Lett.* 2018, *20*, 3300−3304.
(35) Jin, Z.; Teo, Y. C.; Teat, S. J.; Xia, Y. Iterative Synthesis of Edge-Bent [3]Naphthylene. *Synlett* 2018, *29*, 2547−2551.
(36) Jin, Z.; Yao, Z.-F.; Barker, K. P.; Pei, J.; Xia, Y. Dinaphthobenzo[1,2:4,5]dicyclobutadiene: Antiaromatic and Orthogonally Tunable Electronics and Packing. *Angew. Chem., Int. Ed.* 2019, *58*, 2034−2039.
(37) Wu, X.; Zhou, J. An efficient method for the Heck−Catellani reaction of aryl halides. *Chem. Commun.* 2013, *49*, 11035−11037.
(38) Fujise, K.; Tsurumaki, E.; Fukuhara, G.; Hara, N.; Imai, Y.; Toyota, S. Multiple Fused Anthracenes as Helical Polycyclic Aromatic Hydrocarbon Motif for Chiroptical Performance Enhancement. *Chem. - Asian J.* 2020, *15*, 2456−2461.
(39) Hirshfeld, F. L.; Sandler, S.; Schmidt, G. M. J. 398. The structure of overcrowded aromatic compounds. Part VI. The crystal structure of benzo[c]phenanthrene and of 1,12-dimethylbenzo[c]-phenanthrene. *J. Chem. Soc.* 1963, 2108−2125.
(40) Krygowski, T. M.; Cyranski, M. Separation of the energetic and geometric contributions to the aromaticity. Part IV. A general model for the π-electron systems. *Tetrahedron Lett.* 1996, *52*, 10255−10264.
(41) Krygowski, T. M.; Cyranski, M. K. Structural Aspects of Aromaticity. *Chem. Rev.* 2001, *101*, 1385−1420.

https://doi.org/10.1021/jacs.2c02457
J. Am. Chem. Soc. 2022, 144, 12715−12724